

# CoRoT 102699796, the first metal-poor Herbig Ae pulsator: a hybrid $\delta$ Sct- $\gamma$ Dor variable?<sup>\*†</sup>

V. Ripepi<sup>1‡</sup>, F. Cusano<sup>1</sup>, M. Di Criscienzo<sup>2</sup>, G. Catanzaro<sup>3</sup>, F. Palla<sup>4</sup>,  
M. Marconi<sup>1</sup>, P. Ventura<sup>2</sup>, C. Neiner<sup>5</sup>, C. Catala<sup>5,6</sup>, S. Bernabei<sup>6</sup>

<sup>1</sup>INAF-Osservatorio Astronomico di Capodimonte, I-80131, Napoli, Italy

<sup>2</sup>INAF-Osservatorio Astronomico di Roma, I-00040, Roma, Italy

<sup>3</sup>INAF-Osservatorio Astrofisico di Catania, I-95123, Catania, Italy

<sup>4</sup>INAF-Osservatorio Astrofisico di Arcetri, I-50125, Firenze, Italy

<sup>5</sup>LESIA, Observatoire de Paris, CNRS, UPMC, Université Paris Diderot, 92190 Meudon, France

<sup>6</sup>INAF-Osservatorio Astronomico di Bologna, I-40127, Bologna, Italy

## ABSTRACT

We present the analysis of the time series observations of CoRoT 102699796 obtained by the CoRoT satellite that show the presence of five independent oscillation frequencies in the range 3.6–5 c/d. Using spectra acquired with FLAMES@VLT, we derive the following stellar parameters: spectral type F1V,  $T_{\text{eff}}=7000\pm 200$  K,  $\log(g)=3.8\pm 0.4$ ,  $[M/H]=-1.1\pm 0.2$ ,  $v\sin i=50\pm 5$  km/s,  $L/L_{\odot}=21_{-11}^{+21}$ . Thus, for the first time we report the existence of a metal poor, intermediate-mass PMS pulsating star. Ground-based and satellite data are used to derive the spectral energy distribution of CoRoT 102699796 extending from the optical to mid-infrared wavelengths. The SED shows a significant IR excess at wavelengths greater than  $\sim 5\mu$ . We conclude that CoRoT 102699796 is a young Herbig Ae (F1Ve) star with a transitional disk, likely associated to the HII region [FT96]213.1–2.2.

The pulsation frequencies have been interpreted in the light of the non-radial pulsation theory, using the LOSC code in conjunction with static and rotational evolutionary tracks. A minimization algorithm was used to find the best-fit model with  $M=1.84 M_{\odot}$ ,  $T_{\text{eff}}=6900$  K which imply an isochronal age of  $t\sim 2.5$  Myr. This result is based on the interpretation of the detected frequencies as  $g$ -modes of low-moderate  $n$ -value. To our knowledge, this is the first time that such modes are identified in an intermediate-mass PMS pulsating star. Since CoRoT 102699796 lies in the region of the HR diagram where the  $\delta$  Sct and  $\gamma$  Dor instability strips intersect, we argue that the observed pulsation characteristics are intermediate between these classes of variables, i.e. CoRoT 102699796 is likely the first PMS hybrid  $\gamma$  Dor- $\delta$  Sct pulsator ever studied.

**Key words:** stars: pre-main-sequence – stars: variables: T Tauri, Herbig Ae/Be – stars: variables:  $\delta$  Scuti – stars: fundamental parameters – stars: abundances – infrared: stars.

## 1 INTRODUCTION

Asteroseismology of Herbig Ae stars offers a unique means to probe their interior structure and to compare to evolutionary models. It is now well established that these stars during contraction towards the main sequence cross the instability strip of more evolved stars. These young, pulsating intermediate-mass stars are collectively called PMS  $\delta$  Sct and their variability is characterized by short periods ( $\sim 30\text{m}\div 5$  h) and small amplitudes (from less than a millimag to a few hundredths of magnitude, see, e.g.

<sup>\*</sup> The CoRoT space mission, launched on December 27th 2006, has been developed and is operated by CNES, with the contribution of Austria, Belgium, Brazil, ESA (RSSD and Science Programme), Germany and Spain.

<sup>†</sup> Based on observations collected at the European Southern Observatory, Paranal, Chile. Proposal n. 082.D-0839A

<sup>‡</sup> E-mail: ripepi@oacn.inaf.it

Kurtz & Marang 1995; Catala 2003; Ripepi et al. 2006; Zwintz 2008).

The first theoretical investigation of the PMS instability strip based on nonlinear convective hydrodynamical models was carried out by Marconi & Palla (1998), who calculated its topology for the first three radial modes. These authors also found that the interior structure of PMS stars crossing the instability strip is significantly different from that of more evolved Main Sequence stars (with the same mass and temperature), even though the envelope structures are similar. The subsequent theoretical work by Suran et al. (2001) made a comparative study of the seismology of a 1.8 PMS and post-MS star. They found that the unstable frequency range is roughly the same for PMS and post-MS stars, but that some non-radial ( $g$ ) modes are very sensitive to the deep internal structure. More recently, Grigahcène et al. (2006) produced a theoretical instability strip for PMS stars for the first seven radial modes; Ruoppo et al. (2007) derived a model based relation between the large frequency separation and the stellar luminosity and effective temperature and developed a tool to compare theory and observations in the echelle diagram. Finally Di Criscienzo et al. (2008) applied the ATON evolutionary code to the computation of detailed grids of standard (non-rotating) and rotating pre-main sequence (PMS) models and computed their adiabatic oscillation spectra.

From the observational point of view, multi-site campaigns (e.g., Ripepi et al. 2003; Bernabei et al. 2009) and space observations with MOST (e.g., Zwintz et al. 2009, for NGC2264) provided us with good sets of frequencies to be compared with the models. In addition, spectroscopic studies (see, e.g. Fumel & Böhm 2008; Böhm et al. 2009, for the cases of HD104237 and RS Cha, respectively) demonstrated to be very valuable for line profile analysis and direct mode determination using tools like F2D (Kennelly 1994; Kennelly & Walker 1996) or FAMIAS (Zima 2008). However, the full exploitation of the PMS  $\delta$  Sct instability strip is still far from being realized. Dedicated observations of a large sample of PMS stars covering the whole instability strip are needed to accomplish this goal.

In this context, a fundamental contribution can be provided by the data coming from the space telescope CoRoT (*Convection, Rotation and planetary Transits*; Baglin et al. 2007). This satellite took images of the same region of the sky for about five consecutive months reaching relatively faint stars (up to  $V \sim 15$  mag) in its “exo field”, with good precision and very high duty cycle. Particularly interesting was the first long-term pointing of CoRoT, the so-called “Long Run a1” (*LRa1*) which imaged a region of the sky in the galactic anti-center where a few distant Star Forming Regions (SFR) are present.

With the aim of searching for possible PMS  $\delta$  Sct variables present in the CoRoT data, we have studied all the stars identified as  $\delta$  Sct from the CoRoT variable star classification group (Debosscher et al. 2009), looking at near infrared (NIR) excess and emission in the Balmer lines, i.e. typical features of PMS objects. We mainly used the 2MASS photometry (Skrutskie et al. 2006) and the yet unpublished FLAMES@VLT spectroscopic survey of CoRoT variables in *LRa1* performed by C. Neiner and collaborators (ESO proposal 082.D-0839A). Among the about 76 stars classified as  $\delta$  Sct with available spectrum observed by CoRoT

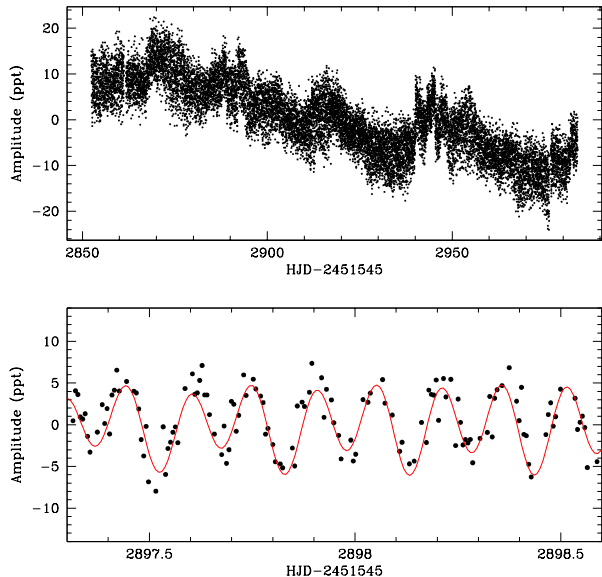


**Figure 1.** Upper panel: light curve of CoRoT 10269979 before detrending (see text). Lower panel: selected portion of the light curve after detrending with overimposed the least-square fit (solid line) to the data obtained with the five “genuine” frequencies (see Sect. 2.2).

during *LRa1*, the only candidate PMS  $\delta$  Sct variable was CoRoT 102699796, a relatively faint star with  $V=15.51$  mag, located in the direction of Monoceros (RA,DEC 06:43:38.46 –01:07:46.7, J2000). This paper is devoted to a complete characterization of this star on the basis of time-series CoRoT observations and a variety of additional data, such as VLT mid-resolution spectroscopy and optical-NIR ground-based, as well as space infrared photometry.

In sections 2 and 3 we present the CoRoT photometry and the VLT spectroscopy, respectively. In section 4 we discuss the evolutionary status of CoRoT 102699796 and its possible membership to the Star Forming Region [FT96]213.1-2.2. In section 6 we interpret the observed oscillation frequencies to the light of non-radial pulsation theory; a summary of the major findings of present work closes this paper.

## 2 PHOTOMETRIC OBSERVATIONS WITH COROT

CoRoT 102699796 was observed by the CoRoT satellite in its “exo field” during the Galactic anti-centre *LRa1* run, between October 27, 2007 and March 3, 2008. The data span about 131.5 consecutive days. The exposure time was of 512 seconds. We used the data corrected to the N2 level (the processing steps are described in Auvergne et al. 2009), which contains 22036 flux measurements. The first step of data processing consisted in removing all the points with non-0 flag (Auvergne et al. 2009), i.e. mainly removing those measurements heavily affected by the transit through the South Atlantic Anomaly (SAA). A few obvious outliers were rejected, too. The resulting light curve was trans-

formed in part-per-thousand (ppt hereafter) using the formula  $1000 \times [(\text{flux}/\text{average}) - 1]$ , where *average* is the mean over the whole light curve. This procedure left us with 14997 useful data points which are shown in Fig. 1 (upper panel). The light curve clearly shows a monotonic dimming probably due to the ageing of the CCD and/or optics of CoRoT, as well as shorter time scale variability, of the order of  $\sim 15$ -30 d and  $\sim 3$ -5 d. The former “periodicity” could be ascribed to variable dust obscuration due to the passing of circumstellar material in front of the star (see, e.g. van den Ancker et al. 1998), whereas the latter could be due to rotational modulation related to coronal activity (see, e.g. Catala 2003). However, given that the observed amplitudes are of only 1-2 hundredths of magnitudes for both types of variability, we cannot exclude that all these long term variation are due to instrumental effects. Moreover, the light curve also appears affected by small “steps”, i.e. sudden jumps in brightness of instrumental origin, common among the CoRoT light curves in the “exo field” field (see, e.g. Mislis et al. 2010). This occurrence makes it difficult to understand whether a feature is intrinsic or due to instrumental problems. To get rid of this effect, we decided to apply a high-pass filter to the light curve, removing all the long-term variability by filtering out all the frequencies lower than 0.50 c/d (all the periods larger than 2 days). This very simple approach is effective in removing also the quoted “steps” because they are not particularly strong in our case, and no specific treatment is needed. We emphasize that the above procedures modify the variability features of the star at frequencies much lower than those typical of the expected  $\delta$  Sct pulsation, therefore, they do not affect at all the frequency analysis which is presented in the next section.

## 2.1 Frequency analysis

The pulsation frequency analysis was carried out with the *period04* package (Lenz & Breger 2005), which adopts both Fourier and least squares algorithms, and permits the simultaneous fitting of multiple sinusoidal variations, and thus does not rely on sequential prewhitening. We have also used, for comparison purposes, the *SigSpec* package, which follows a different approach (Reegen 2007).

First, we calculated the spectral window (SW) of the data up to the Nyquist frequency ( $\sim 84$  c/d), as shown in panel a) of Fig. 2. The SW shows several features due to the satellite’s orbital period of about 7000 s (variable up to four seconds), and its multiples. This is due to the removal of data points during the passage through the SAA. Moreover, since the scattered light falling on the detector varies during the orbit of the satellite, the periodogram of the star is expected to present the orbital period ( $\sim 13.96$  c/d) with the relative aliases and harmonics. Frequencies close to these values will be rejected in the following analysis.

The Fourier transform of the data is shown in panel b) of Fig. 2. It can be seen that there is a dominant frequency at about 6.55 c/d and other signal up to the Nyquist frequency. Most of the signal is represented by the aliases of the dominant frequency and is removed by the prewhitening procedure. We extracted frequencies with *period04* using as a limit for the last significant frequencies the widely used empirical criteria of  $S/N=4$  (Breger et al. 1993). To estimate the noise, following well established procedures (see,

e.g. Rodríguez et al. 2006; García Hernández et al. 2009), we calculated the average amplitude of the residuals (after prewhitening all the significant peaks) in a frequency interval of width=5 c/d centred on the corresponding peak. Quantitatively the noise resulted to be quite flat beyond  $\sim 1$  (c/d) with an average value  $\sim 0.03$  (ppt). In this way we were able to extract 15 significant frequencies. Among these, four (at 27.9416, 41.91337, 27.9379, and 13.9617 c/d) are related to the orbital period of the satellite and will be ignored in the analysis. The remaining eleven frequencies are listed in the first three columns of Table 1 together with the amplitude and S/N. The same procedure was carried out with *SigSpec*, obtaining the same results, as shown in Table 1 where *sig* represent the spectral significance (see Reegen 2007, for an explanation). Following Reegen (2007); Kallinger, Reegen, & Weiss (2008), a value of *sig*=5.46 should be approximately equivalent to  $S/N=4.0$ . However, as shown in Tab 1, in our case this S/N value corresponds to a *sig*  $\sim 6.6$ . The origin of such a discrepancy, which was already found by other Authors in the literature, is not clear. A detailed discussion about this occurrence is beyond the scope of present paper, indeed our results are not affected at all, since our main discriminant for the significant frequencies remains the  $S/N=4.0$  criterion. However, the interested reader can consult e.g. García Hernández et al. (2009) for a discussion on this subject.

As a further check on the reliability of the frequency extraction, we analysed separately selected portions of the time-series, with a size of about 10-15 d, and dealing with both “detrended” and raw data (in this case avoiding portions including “steps”). All the relevant frequencies were found in all the cases, reinforcing our confidence about the reliability of the results presented here.

The precision on the single frequencies is also given in Table 1. It has been estimated adopting the definition by Kallinger, Reegen, & Weiss (2008) :  $\sigma f = 1/(T\sqrt{\text{sig}(A)})$ , where  $T$  is the duration of the time-series and *sig*( $A$ ) is the significance of the frequency with amplitude  $A$  as calculated by *SigSpec*. We also report the uncertainty on the frequencies on the basis of the Rayleigh criterion  $(1/4T)^{1/2} = 0.002$  c/d. This more conservative estimate (at 3- $\sigma$  level) is the value used for the comparison to the theoretical models.

## 2.2 Combination of frequencies

Linear combinations of the terms having the highest amplitudes have been observed in low-amplitude  $\delta$  Sct stars both from the ground and from space (see, e.g. Breger et al. 2005; Poretti et al. 2009). To search for possible combinations among the frequencies observed in CoRoT 102699796, we decided to use the *Combine* package, an ad hoc computer program written by P. Reegen. This program checks one frequency after the other for being a linear combination of previously examined frequencies. If this attempt fails, the corresponding frequency is considered “genuine”. Only genuine frequencies are used to form linear combinations subsequently (see Reegen 2010, for a detailed description). Applying this package to the investigated star, we find only

<sup>1</sup> see Kallinger, Reegen, & Weiss (2008) and references therein for a discussion about this definition

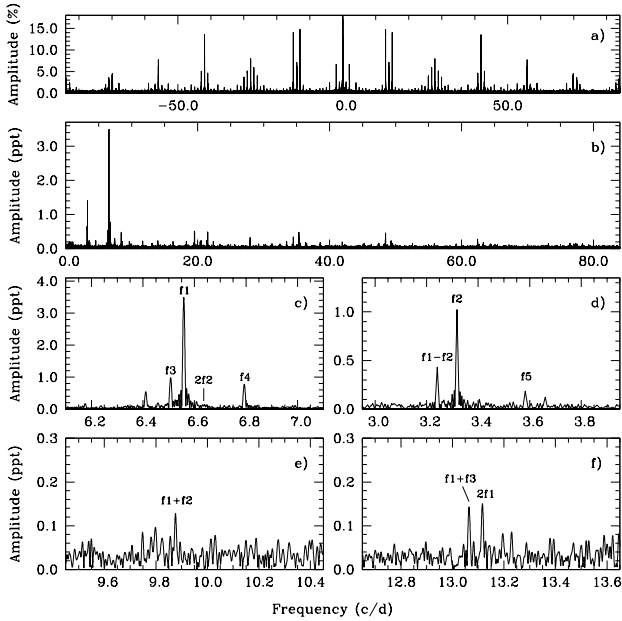


**Figure 2.** Panel a): spectral window of the data up to the Nyquist frequency. Panel b): Fourier Transform of the data. Panels c) to f): enlargements of Panel b) showing the relevant peaks extracted from the periodogram. Labels are the same as in Table 1.

five genuine frequencies. All the other frequencies can be explained as simple linear combination of these terms. We varied the input parameters of Combine to verify the robustness of the combination calculation. The genuine and the combination frequencies are identified in the last column of Table 1 and in the periodograms of panels c) to f) of Fig. 2.

### 3 SPECTROSCOPIC OBSERVATIONS

Intermediate-resolution spectroscopy of CoRoT 102699796 was carried out with *Fibre Large Area Multi-Element Spectrograph (FLAMES)*, (Pasquini et al. 2002) mounted at the Nasmyth A platform of the VLT 8.2-m unit telescope 2. The low-resolution gratings *LR02* and *LR06* were used, leading to a resolving power of  $R \approx 6400$  and  $R \approx 8600$ , respectively. The spectral range coverage is about 600 Å (3960 – 4560 Å) for the blue grating and about 700 Å (6440 – 7160 Å) for the red grating.

We acquired four exposures with the *LR02* grating, two during the night of 2009, February 09 and two others during the night 2009, March 22. In order to increase the signal-to-noise ratio of the final spectrum, we corrected each single spectrum to the velocity restframe, we verified that no residual lines shift is present at our resolution (i. e., due to a hidden companion), and finally we combined all of them in one spectrum with a total exposure time of 2160 sec, and a SNR of  $\sim 60$ .

Only one exposure has been obtained using the *LR06* grating, precisely during the night 2009, February 09, with an exposure time of 2400 sec and with a SNR of  $\approx 40$ .

For the following analysis we used the 1-D, wavelength-

calibrated spectra as reduced by the dedicated Giraffe pipeline<sup>2</sup>.

### 3.1 Spectral type and atmospheric parameters

#### 3.1.1 Determination of effective temperature

Any attempt devoted to a detailed characterization of the chemical abundance pattern in stellar atmospheres relies on the accuracy of effective temperature and surface gravity determination.

In this study, we derived the effective temperature by using the ionization equilibrium criterion. In practice, we adopted as  $T_{\text{eff}}$  the value that give the same iron abundance as computed from a sample of spectral lines (both neutral and first ionization stage) present in the spectral range between 4000 Å and 4500 Å (see Tab. 2).

We used the method of the spectral synthesis in order to overpass the strong blending due to relatively high rotational velocity (see below). To perform these calculations we used ATLAS9 (Kurucz 1993) to compute LTE atmospheric models and SYNTHE (Kurucz & Avrett 1981) to reproduce the observed spectrum. Line lists and atomic parameters used in our modeling are from Kurucz & Bell (1995) and the subsequent update by Castelli & Hubrig (2004). From the first steps of our iterative procedure, it appeared that the star has a low metal content. Thus, we decided to use Opacity Distribution Functions [ODF] computed for sub-solar metallicity. At the end we estimated  $T_{\text{eff}} = 7000 \pm 200$  K, computed for ODF  $[M/H] = -1$ . The error on the temperature was estimated to be the the variation in the parameter that increases the  $\chi^2$  by unity.

As a by-product, we obtained an estimate of the projected rotational velocity  $v \sin i = 50 \pm 5$  km/s and an iron abundance  $[Fe/H] = -1.1 \pm 0.2$ . Unfortunately, we were able to obtain only an upper limit for the magnesium abundance  $[Mg/H] \leq -2$ .

In Figs. 3, we show two portions of our spectral range: one including the Balmer lines and the other covering the spectral range 4380 - 4440 Å, respectively, with the synthetic spectra superimposed.

It is worth mentioning that the metallicity measured for CoRoT 102699796 is rather low with respect to that expected on the basis of recent estimates of the Galactic metallicity gradient (see, e.g. Pedicelli et al. 2009, and references therein), i.e.  $[Fe/H] \sim -0.5$ . However, as discussed in Sect.5, it is possible that the region where CoRoT 102699796 formed, is associated with the young open cluster Dolidze 25 and with the star forming complex that include other HII regions (such as Sh 2-284/5), which is known to host stars as metal poor as  $[Fe/H] \sim -0.8$  (Lennon et al. 1990), a value close to that measured for our target star. The reason of such a low metallicity is not clear, and of course needs to be investigated in detail, however this is beyond the scope of the present paper.

<sup>2</sup> BLDRS v0.5.3, written at the Geneva Observatory, see <http://girbltrs.sourceforge.net>

**Table 1.** Pulsation frequencies for CoRoT 102699796. Columns (1)-(4) show frequencies (in c/d and  $\mu$ Hz), amplitudes and S/N derived with *period04*, respectively. Columns (5)-(7) present frequencies, amplitudes and *sig* values obtained with *sigSpec*, respectively. Column (8) show the uncertainty on the frequencies (after Kallinger, Reegen, & Weiss (2008)), whereas column(9) exhibit their identification.

$F_{P04}$ (c/d) (1)	$F_{P04}$ $\mu$ Hz (2)	$A_{P04}$ (ppt) (3)	S/N $_{P04}$ (4)	$F_{SigSpec}$ (c/d) (5)	$A_{SigSpec}$ (ppt) (6)	$Sig_{SigSpec}$ (7)	$\sigma_f$ (c/d) (8)	Identification (9)
6.5584	75.91	3.47	116.5	6.5584	3.47	1585.4	0.0002	f1
3.3180	38.40	1.40	37.9	3.3180	1.40	497.5	0.0003	f2
6.5069	75.31	0.96	32.1	6.5069	0.96	273.4	0.0005	f3
6.7929	78.62	0.76	25.2	6.7929	0.76	186.6	0.0006	f4
3.2405	37.51	0.66	17.6	3.2406	0.66	147.1	0.0006	f1-f2
3.5822	41.46	0.23	6.5	3.5822	0.23	19.2	0.0017	f5
3.6603	42.36	0.18	5.2	3.6603	0.18	12.4	0.0022	2f2-f1
13.1164	151.81	0.15	4.9	13.1162	0.16	8.8	0.0026	2f1
13.0645	151.21	0.14	4.7	13.0646	0.14	7.7	0.0027	f1+f3
6.6361	76.81	0.13	4.3	6.6366	0.13	7.0	0.0029	2f2
9.8762	114.31	0.13	4.1	9.8761	0.13	6.6	0.0030	f1+f2

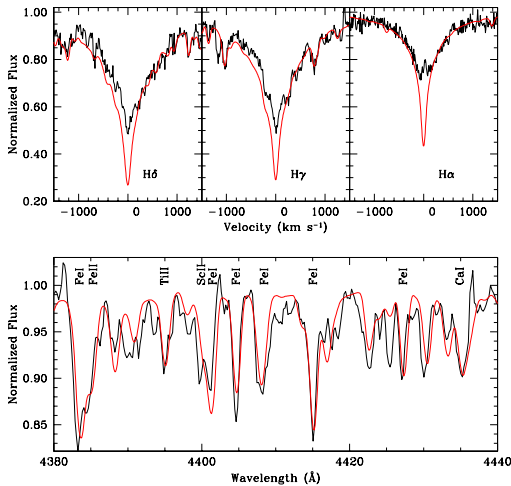


**Figure 3.** Top and bottom panels show selected portions of our spectrum, i.e., the Balmer lines and the 4380-4440 Å range, respectively. In both panels the synthetic spectra is overimposed (red line).

### 3.1.2 Determination of surface gravity and luminosity

For early F-type stars, one of the method commonly used in the literature for the determination of the luminosity class of stars is through the strength of the ratios between the spectral blend at  $\lambda\lambda$  4172-4179 Å, mostly FeII and TiII lines, and that at  $\lambda$ 4271 Å, mostly composed of Fe I lines (Gray & Garrison 1989).

We computed the  $\lambda\lambda$  4172-4179/4271 ratio which resulted in  $1.60 \pm 0.15$ , roughly corresponding to a luminosity class of V (Gray & Garrison 1989).

To derive the surface gravity of our target, we computed the theoretical behavior of the above ratio as a function of  $\log g$ . After having fixed  $T_{\text{eff}}$  to the value found in Sect. 3.1.1, we computed a grid of ATLAS9 atmospheric models with gravities spanning the range between 3.0 and 4.5 dex. The theoretical equivalent widths and consequently

**Table 3.** Physical parameters of CoRoT 102699796 as derived from spectroscopy.

SpT	$T_{\text{eff}}$ (K)	$\log(g)$	[M/H]	$v \sin i$ (km/s)	L ( $L_{\odot}$ )
F1V	$7000 \pm 200$	$3.8 \pm 0.4$	$-1.1 \pm 0.2$	$50 \pm 5$	$21^{+21}_{-11}$

the ratio  $\lambda\lambda$  4172-4179/4271, have been evaluated using the code XLINOP (Kurucz & Avrett 1981). By using this curve, we converted our measured ratio and its associated error in a measurement of gravity and of its uncertainty, obtaining:  $\log g = 3.8 \pm 0.4$ .

Using the above results, we conclude that CoRoT 102699796 has spectral type F1 V.

The atmospheric parameters derived here can be used to estimate the stellar luminosity. To this aim, we use the approach by Balona et al. (2011). Starting from the Stefan-Boltzmann law  $L=L(T_{\text{eff}},R)$  where R is the radius and all the quantities are in solar units, we can eliminate the radius from the definition of gravity  $g=g(R,M)$ , where M is the mass, obtaining a relation  $L=L(T_{\text{eff}},M,g)$ . Finally, the mass can be eliminated using the empirical mass-luminosity relation by Malkov (2007):  $\log L/L_{\odot} = \log(M/M_{\odot}) = 0.00834 + 0.213 \log(L/L_{\odot}) + 0.0107 \log(L/L_{\odot})^2$ , thus deriving the desired  $L=L(T_{\text{eff}},g)$  relation.

By using this relation we obtain  $\log(L/L_{\odot})=1.33 \pm 0.3$  for CoRoT 102699796. The relevant stellar parameters for this star are shown in Table 3.

In Figs. 3, we show two portions of our spectral range: one including the Balmer lines and the other covering the spectral range 4380-4440 Å, respectively. The synthetic spectra superposed has been calculated using the atmospheric parameters derived as described before and summarized in Tab. 3.

**Table 2.** Neutral and first ionization state iron lines identified in the range 4000 - 4500 Å for CoRoT 102699796, used for effective temperature and iron abundance calculation. For each line we report wavelength and oscillator strength.

$\lambda$	$\log gf$	El	$\lambda$	$\log gf$	El	$\lambda$	$\log gf$	El
4001.661	-1.880	FeI	4143.415	-0.204	FeI	4250.119	-0.405	FeI
4002.083	-3.471	FeII	4143.868	-0.450	FeI	4250.787	-0.710	FeI
4005.242	-0.610	FeI	4147.669	-2.104	FeI	4258.154	-3.400	FeII
4007.272	-1.300	FeI	4153.900	-0.270	FeI	4260.474	-0.020	FeI
4009.713	-1.200	FeI	4154.499	-0.688	FeI	4271.153	-0.349	FeI
4014.531	-0.200	FeI	4154.805	-0.370	FeI	4271.760	-0.164	FeI
4017.148	-0.920	FeI	4156.799	-0.620	FeI	4273.326	-3.258	FeII
4021.866	-0.660	FeI	4157.780	-0.403	FeI	4278.159	-3.816	FeII
4024.725	-0.710	FeI	4158.792	-0.670	FeI	4282.403	-0.810	FeI
4030.488	-0.555	FeI	4170.901	-1.100	FeI	4294.125	-1.110	FeI
4032.627	-2.440	FeI	4173.461	-2.180	FeII	4296.572	-3.010	FeII
4043.897	-0.826	FeI	4174.913	-2.969	FeI	4299.234	-0.430	FeI
4044.609	-1.080	FeI	4175.636	-0.670	FeI	4303.176	-2.490	FeII
4045.594	-0.896	FeI	4176.566	-0.620	FeI	4307.902	-0.070	FeI
4045.812	0.280	FeI	4177.692	-3.753	FeII	4314.310	-3.477	FeII
4062.441	-0.780	FeI	4178.862	-2.480	FeII	4315.085	-0.970	FeI
4063.276	-0.748	FeI	4180.981	-1.840	FeII	4325.762	-0.010	FeI
4063.594	0.070	FeI	4181.755	-0.180	FeI	4351.769	-2.100	FeII
4066.974	-0.856	FeI	4184.891	-0.860	FeI	4352.735	-1.260	FeI
4067.271	-1.419	FeI	4187.039	-0.548	FeI	4369.411	-3.670	FeII
4067.978	-0.430	FeI	4187.795	-0.554	FeI	4369.772	-0.730	FeI
4070.770	-0.790	FeI	4191.430	-0.666	FeI	4375.930	-3.031	FeI
4071.738	-0.022	FeI	4195.329	-0.492	FeI	4383.545	0.200	FeI
4073.762	-0.920	FeI	4198.247	-0.456	FeI	4384.319	-3.500	FeII
4074.786	-0.970	FeI	4198.304	-0.719	FeI	4385.387	-2.570	FeII
4075.954	-3.380	FeII	4199.095	0.250	FeI	4404.750	-0.142	FeI
4076.629	-0.360	FeI	4202.029	-0.708	FeI	4413.601	-3.870	FeII
4078.354	-1.500	FeI	4203.938	-0.350	FeI	4415.122	-0.615	FeI
4081.567	-0.200	FeI	4210.343	-0.870	FeI	4416.830	-2.600	FeII
4084.492	-0.590	FeI	4216.183	-3.356	FeI	4427.310	-3.044	FeI
4085.004	-1.280	FeI	4217.546	-0.510	FeI	4442.339	-1.255	FeI
4085.303	-0.710	FeI	4219.360	0.120	FeI	4447.717	-1.342	FeI
4114.445	-1.220	FeI	4222.213	-0.967	FeI	4459.117	-1.279	FeI
4118.545	0.280	FeI	4224.171	-0.410	FeI	4461.653	-3.210	FeI
4121.802	-1.300	FeI	4225.454	-0.500	FeI	4466.551	-0.590	FeI
4122.668	-3.380	FeII	4227.427	0.230	FeI	4472.929	-3.430	FeII
4127.608	-0.990	FeI	4233.172	-2.000	FeII	4476.019	-0.570	FeI
4128.748	-3.760	FeII	4233.602	-0.604	FeI	4482.170	-3.501	FeI
4132.058	-0.650	FeI	4235.936	-0.341	FeI	4482.253	-1.482	FeI
4132.899	-0.920	FeI	4238.810	-0.280	FeI	4489.183	-2.970	FeII
4134.677	-0.490	FeI	4245.258	-1.170	FeI	4491.405	-2.700	FeII
4136.998	-0.540	FeI	4247.425	-0.230	FeI	4494.563	-1.136	FeI

#### 4 THE EVOLUTIONARY STATUS OF COROT 102699796

In this section we deal with the evolutionary status of our target: is it indeed a young intermediate-mass star (Herbig Ae type), as we suspect? We have seen in the previous section that the Balmer lines in the spectrum appear to be filled. This is the first necessary clue. The next steps are to investigate if 1) the star shows infrared excess, and 2) it is possible to associate it with a known star forming region.

##### 4.1 The SED of CoRoT 102699796

We start by building the Spectral Energy Distribution (SED) for CoRoT 102699796. A set of photometric data was

collected from the literature. Observations in the  $B, V, R$  and  $I$  Johnson bands are present in the CoRoT EXO-dat catalogue (Deleuil et al. 2009). The NIR data in the  $J, H,$  and  $K$  bands were taken from the 2MASS catalog (Skrutskie et al. 2006; Cutri et al. 2003). Four measurements in the mid- and far-infrared were collected from the AKARI Infrared Astronomical Satellite catalogues IRC (mid-IR all-sky Survey, Ishihara et al. 2010) and FIS (Far-IR all-sky Survey, Yamamura et al. 2010). The data were acquired by the Akari-satellite in four bands centered on 9, 18, 65 and 90  $\mu\text{m}$ . The position accuracy in the first two bands is estimated to be better than  $2''$ . At larger wavelengths the pixel size is of  $26.8''$  and the average position disagreement between the AKARI-FIS catalogue and the Simbad catalogue is of  $\sim 6.5$  arcsec. The source identified in the AKARI-FIS catalogue

is at a distance of  $\sim 23$  arcsec from the coordinates given in the CoRoT catalogue for CoRoT 102699796. Given the pixel sizes of the AKARI camera and the absence of bright sources in a radius of 23 arcsec around CoRoT 102699796, we can state that the observed FIR flux comes from this star. Additional data in the mid-IR can be retrieved from the database of the mission Midcourse Space Experiment (MSX) (Egan et al. 2003). In particular, the target star was detected in the *A* band of the satellite (centered at  $8.28 \mu$ ), which is close in wavelength to the AKARI *S9W* band. Note that these two independent measures are in perfect agreement one each other (see Fig. 4).

The magnitudes of the star were dereddened by using the relations given in Cardelli et al. (1989) between the  $A_v$  and the other photometric bands. In order to estimate  $A_v$ , we compared the  $B - V$ ,  $V - I$  and  $V - R$  colours with the ones obtained using the stellar models of Castelli et al. (2004) for the temperature and the metallicity of the star. The  $E(B-V)$ ,  $E(V-R)$  and  $E(V-I)$  so far derived were then converted to  $A_v$  using the transformations of Cardelli et al. (1989) and averaged. The estimated extinction is  $A_v = 0.93 \pm 0.06$  mag.

The dereddened SED was compared to theoretical models of star+disk computed using the software *cgplus*, a modeling program, written by C.P. Dullemond, for dusty circumstellar disks, based on the models of (Chiang & Goldreich 1997) and (Dullemond et al. 2001). The basic idea is to model the disk around Herbig Ae/Be stars with a passive, irradiated disk with an inner hole. In our case the model which best fit the SED is the one with the parameters reported in Table 4. The SED with the model fit is shown in Fig. 4. We note that the luminosity obtained from the integration of the star's SED is in excellent agreement with that estimated from the spectroscopy, as reported in Tab. 3 (see next section for a discussion about the distance of the target).

The shape of the SED is typical of transitional circumstellar disks (Calvet et al. 2005). These usually have an inner region which is depleted of gas and dust and an outer region which is optically thick. The strong flux rise around  $10 \mu\text{m}$  is presumably due to the frontal illumination of the wall of the optically thick outer disk. Following the classification scheme of Sartori et al. (2010) for Herbig Ae/Be stars, CoRoT 102699796 can be identified as a group 2 object, intermediate between embedded objects and stars with more evolved dusty disks. These group 2 objects can show a doubly peaked SED related to a visible central star (first peak) surrounded by a significant amount of circumstellar cold matter responsible for the second peak in the mid- to far-IR band. In the group 2 objects of Sartori et al. (2010) the second peak is similar to the first, like in the case of CoRoT 102699796 (see Fig. 4).

## 5 MEMBERSHIP

CoRoT 102699796 is placed at an angular distance of 1.65 arcmin from the center of the HII region [FT96]213.1-2.2 (Fich & Terebey 1996) which extends over 9 arcmin in the Monoceros constellation. Moreover Avedisova (2002) lists 7 young objects close ( $\leq 4$  arcmin) to CoRoT 102699796. We believe, indeed, that the CoRoT object, together with the

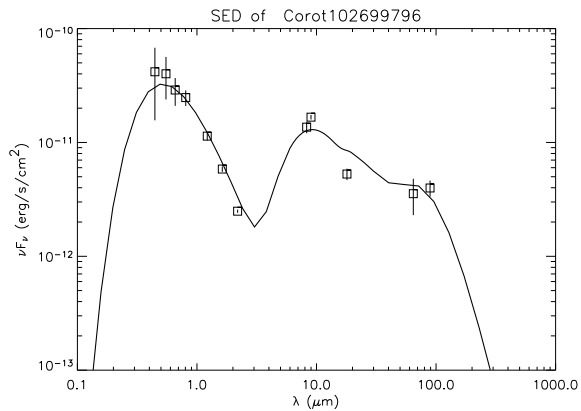


**Figure 4.** The dereddened SED of CoRoT 102699796 is shown with open squares. The continuum line is the total flux given by the model star+disk with the parameters presented in Table 4.

**Table 4.** Parameters derived by the SED fit.

Parameter	value
Distance	4000 pc
Inclination	$60.0^\circ$
Star mass	$2.0 M_\odot$
Star luminosity	$20.0 L_\odot$
Inner disk-radius	4.0 AU
Outer disk-radius	400 AU
Disk mass	$0.06 M_\odot$
Inner disk-temperature	450 K
Surface density exponent	-2.0

7 young objects, belongs to the [FT96]213.1-2.2 HII region, which is in turn associated with a big star formation structure composed by several HII regions, such as Sh 2-284, Sh 2-283 and Sh 2-285 (Russeil et al. 2007). The distance estimate of this structure is still controversial. Russeil et al. (2007) derived, using also data from literature, a distance of 7.89 kpc. Nonetheless one of the biggest part of the star formation structure, the HII region Sh 2-284, was found to be at a distance of 4 kpc by Cusano et al. (2011), in agreement within the errors with the distance of 3.6 kpc given by Delgado, Djupvik & Alfaro (2010). Furthermore, Rolleston et al. (1994) also found that two B0V stars in Sh 2-285 are at a distance of 4.3 kpc. These results combined together, place the star formation region at a distance of 4-4.5 kpc, closer than the estimate of Russeil et al. (2007). The luminosity of CoRoT 102699796 derived by the frequency analysis (as estimated in Sect 6.2), by the spectroscopic observations and by the SED fitting (see Section 4.1), is also compatible with a distance of the object of 4 kpc. The three colour image shown in Figure 5, obtained by combining IRAS images at 25, 60 and  $100 \mu\text{m}$ , illustrates the different components of this large star forming complex. The white open circles are HII regions from the Sharpless (1959) catalogue, while the green circle-square symbols show young

stellar objects from Avedisova (2002). CoRoT 102699796 is inside the circle of [FT96]213.1-2.2.

In the spectroscopic analysis, CoRoT 102699796 was found to have a metallicity very similar to that of Sh 2-284, supporting the assumption of a common origin of the [FT96]213.1-2.2 and Sh 2-284 HII regions. If confirmed, this complex has one of the lowest metallicity galactic known SFRs.

## 6 INTERPRETATION OF THE OBSERVED OSCILLATION FREQUENCIES

### 6.1 Calculation of asteroseismic models

The model analysis performed in this paper is described in detail in Di Criscienzo et al. (2008), and was originally suggested by Guenther & Brown (2004). In summary, given the observed  $N$  frequencies of the investigated star, we look for models having  $\chi^2 \leq 1$  within our grid of oscillation spectra, with the following definition of  $\chi^2$

$$\chi^2 = \frac{1}{N} \sum_{i=1}^N \frac{(f_{obs,i} - f_{mod,i})^2}{\sigma_{obs,i}^2 + \sigma_{mod,i}^2} \quad (1)$$

where  $f_{obs,i}$  and  $f_{th,i}$  are the observed and the model frequency for the  $i$ th mode, respectively, characterized by an observational  $\sigma_{obs,i}$  and a theoretical  $\sigma_{th,i}$  uncertainty. In general, the search for the best-fitting model (corresponding to the oscillation spectrum that minimizes the  $\chi^2$  value) is concentrated in the subgrid of models with  $T_{eff}$  and  $L/L_{\odot}$  within the error box in  $T_{eff}$  and  $L/L_{\odot}$  of the star. If the program does not find any model matching all the frequencies with  $\chi^2 \leq 1$ , it discards one by one the non-matched frequencies, computes the  $\chi^2$  for the remaining frequencies and searches again for models with  $\chi^2 \leq 1$ . Among the resulting models satisfying the condition  $\chi^2 \leq 1$ , the model with the lowest value of the  $\chi^2$  is the best-fitting one. The grid of PMS models were constructed using the ATON code for stellar evolution (Ventura et al. 1998) in the standard version for asteroseismic applications (D’Antona et al. 2005). The physics of the models are up-to-date and described in detail in Di Criscienzo et al. (2008). The ATON code also allows to include the effects of rotation, according to the formulation by Endal & Sofia (1976), as described in Mendes et al. (1999); Landin et al. (2006). The possibility of accounting for the rotation effects proves to be extremely useful for this analysis, since PMS stars have on average high rotational velocities (Böhm & Catala 1995). In general, what we may determine is the projected velocity  $v \sin i$ , but in this particular case we can derive the true rotational velocity ( $\sim 60$  km/s) from the inclination of the disk, assuming the disk is in the stellar rotation plane, and this can be used to further fix the best fit model.

We stress here that the approach by Endal & Sofia (1976) accounts only for the hydrostatic effects of rotation, neglecting the internal angular momentum redistribution; in this work we use a rigid body rotation. The initial angular momentum of the star is provided as a physical input, and chosen to reproduce the observed surface angular velocity of the star at a given position in the HR diagram.

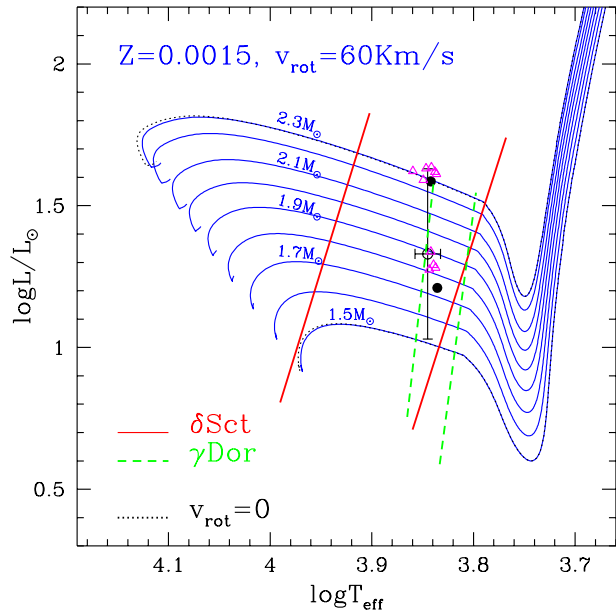


**Figure 6.** HR diagram showing the spectroscopic position of CoRoT 102699796 (open circle) with the respect to several PMS rotational tracks taken from the model grid. The black full circles mark the position of the best fit models found comparing observed and predicted frequencies with  $m=0$  while magenta triangles are the models described in Table 6. The red solid lines and the green dashed lines show the  $\delta$ Sct and  $\gamma$ Dor instability strips by Breger & Pamyatnykh (1998) and Guzik et al. (2000), respectively.

Models were computed from 1.5 to 2.3  $M_{\odot}$ , because these are the masses that enter in the empirical box in the HR diagram (see Fig. 6), with a step of  $\Delta M=0.01 M_{\odot}$ . The evolution begins on the Hayashi track, and the calculation ends when the star has reached the MS. We note that neglecting the protostellar evolution and its effect on the inner structure and pulsation properties does not change the conclusions of the paper because the investigated star lie on the horizontal portion of the PMS evolutionary tracks, subsequent to the thermal relaxing phase undergone by stars around 2  $M_{\odot}$  in the earliest phases of the PMS evolution. The step in effective temperature between consecutive models of the grid is  $\Delta T_{eff} \sim 50$  K.

We use the LOSC oscillation code by Scuflaire et al. (2008) to calculate the frequencies of radial and non radial oscillation modes for each evolutionary structure of the grid. We limit the spherical degree to  $l < 4$  and contrary to previous works on PMS pulsating stars we extend our pulsational analysis also to gravity modes since the oscillation spectra of this star has an anomalous extension to low frequencies suggesting that at least the lowest ones could be low order  $g$ -modes.

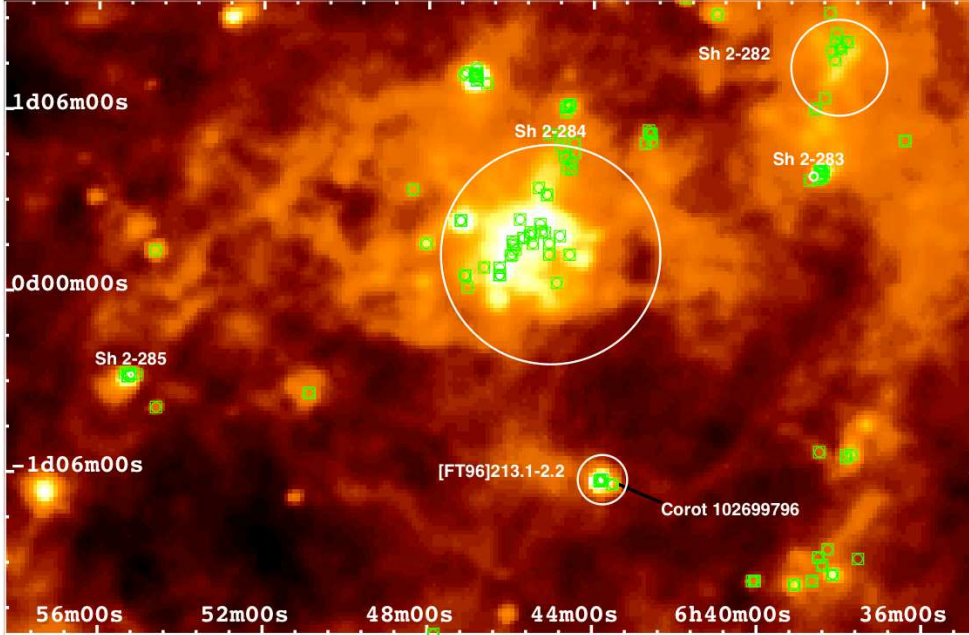


**Figure 5.** Composition of three IRAS image at 25, 60 and 100  $\mu\text{m}$ . White open circles show the HII regions according to the Sharpless (1959) catalogue, while green circle-square symbols show young stellar objects reported by Avedisova (2002). The target star CoRoT 102699796 is inside the circle of [FT96]213.1-2.2.

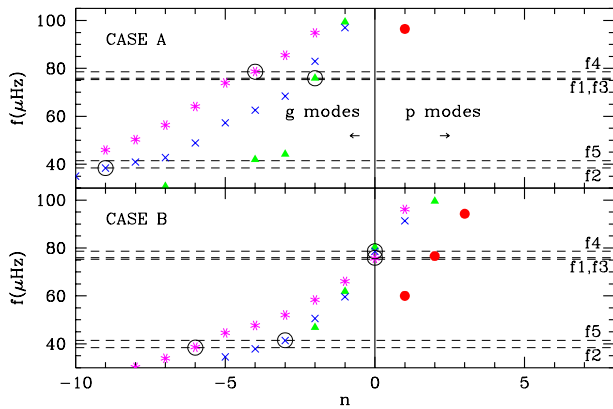


**Figure 7.** Comparison between the observed spectrum of star CoRoT 102699796 and the spectrum of the best fit model obtained in the two cases indicated in Table 5. Filled circles and triangles, crosses and asterisks indicate theoretical frequencies with  $l=0, 1, 2, 3$ , respectively. The open circles indicate the matched frequencies

## 6.2 Comparing observed and predicted frequencies

Among the observed frequencies reported in Table 1 we try to fit those which are not consistent with a linear combination of the others, namely  $f_1$  to  $f_5$ , in the order adopted in Table 1. We also start excluding from the analysis  $f_3$  which is too similar to  $f_1$  and we suggest that these two frequencies are an example of frequency pairs

(separations lower than  $0.7\mu\text{Hz}$  or  $0.06$  c/d) present in the power spectra of the majority of the well-studied  $\delta$  Sct stars, as noted by Breger & Bischof (2002). Since the actual cause for this phenomenon is still unknown we prefer to remove  $f_3$  from our fitting procedure.

In this way we have four observed frequencies to be fitted with computed ones in order to find the best fit model through the  $\chi^2$  analysis.

We assume as uncertainties on observed frequencies in eq. 1 values which are  $3\text{-}\sigma$  the observational errors given in Section 2.1 and consider conservatively theoretical errors of the same order of magnitude of the observational ones, taking into account all the intrinsic numerical uncertainties of models (see Moya 2007, for a detailed quantitative description).

As a result we find that the best fit model corresponds to a very young star ( $t\sim 3$  Myr, with no convective core yet) with  $M=1.74 M_{\odot}$ ,  $T_{\text{eff}}=6850\text{K}$  (CASE A in Table 5). We note that the  $\chi^2$  reported in table is calculated on the basis of the first three frequencies because unfortunately this model does not match frequency  $f_5$ , which however is the one with the lowest S/N ratio (see Tab. 1). Moreover, if we allow  $\chi^2$  to be  $> 1$ , we find that a much more massive model (described in Table 5 as CASE B) minimizes  $\chi^2$ . According to this model, only two frequencies are pure g-mode of low order.

We remark that in the analysis described above the rotation of the star (see Sect. 3) was considered only in the computation of the evolutionary model. For completeness we recall that if  $f$  denotes the frequency in the absence of rotation, a slow solid rotation with angular velocity  $\Omega$  slightly alters the frequency with  $l>0$  in the following way:

$$f_{l,n,m} = f_{l,n} + m\beta_{l,n}\Omega \quad (2)$$

where  $\beta$  is a quantity described in detail in Di Criscienzo et al. (2008) and calculated by the adiabatic oscillation code for each pair (l,n). We then relaxed the previous constraint used to find the best fit model by adding the multiplet (triplet and quintuplet, etc. according to eq. 2) frequencies to our predictions, and we compared again theory and observations using the same technique as above (but this time trying to fit also  $f_3$ ). As a result, the number of best-fitting models grows in number, as shown in Tab. 6, where we list all the models between  $\chi_{min}^2$  and  $\chi_{min}^2 + 1$  (i.e. within  $1 \sigma$ ). However, when we report these models in the HR diagram (empty triangles in Fig. 6), we find out the very interesting result that these models cluster around or close to the two best fit models previously found, namely CASE A and B. This occurrence suggests that models consistently predict two possible solutions for the position of the star in the HR diagram: a) with  $\text{Log}L/L_{\odot} \sim 1.2 \div 1.3$  and  $M/M_{\odot} \sim 1.8$ ; b) with  $\text{Log}L/L_{\odot} \sim 1.6$  and  $M/M_{\odot} \sim 2.3$ . To decide which “class” of models has to be preferred, we note that the “class a)” are the favoured models because: i) they produce the lowest values for the  $\chi^2$  and ii) their luminosities are in better agreement with the values inferred from spectroscopy and from the integration of the SED (although at least formally also the luminosity of class b) models are in agreement with the spectroscopic value at  $1 \sigma$ ). On the basis of the above considerations, our best-fit model is the one that minimize the  $\chi^2$  (model a1 in Tab. 6), with mass, effective temperature and luminosity of  $1.84 M/M_{\odot}$ ,  $6900 \text{ K}$ , and  $1.29 \text{ Log}L/L_{\odot}$ , respectively. Similarly to CASE A, it is a young model ( $\sim 2.5 \text{ Myr}$ ) still without a convective core. It is important to note that the observed frequency spectrum can be interpreted in terms of  $g$ -modes with low-moderate  $n$ -value for class a) models, whereas class b) models are characterized by both  $p$ - and  $g$ -modes.

These results, if confirmed, would be of crucial importance because it would be the first time that  $g$ -modes are detected in a Herbig Ae pulsating star. An even more complicate picture emerges if we consider that CoRoT 102699796 lies (see Fig. 6) in the region of the HR diagram where  $\delta \text{ Sct}$  and  $\gamma \text{ Dor}$  instability strips intersect (at least for solar metallicity, see e.g. Handler & Shobbrook 2002). We recall that the frequency spectrum of  $\gamma \text{ Dor}$  stars is interpreted in terms of high radial order  $g$ -modes. Our findings suggest that CoRoT 102699796 shows a frequency spectrum with intermediate properties between  $\delta \text{ Sct}$  and  $\gamma \text{ Dor}$ , characterized by frequencies lower and higher than those typical of  $\delta \text{ Sct}$  and  $\gamma \text{ Dor}$  variables, respectively. In fact, according to our interpretation this star is a pre-main sequence pulsator which shows  $g$ -modes of low-moderate radial number and order in its frequency spectrum (or both  $p$ - and  $g$ -modes, see above). In this context, it is worth noticing that hybrid  $\delta \text{ Sct}$ - $\gamma \text{ Dor}$  pulsators were already found among more evolved stars by several authors (see, e.g. Henry & Fekel 2005; King et al. 2006; Rowe et al. 2006; Handler 2008). Moreover, the recent data obtained with the KEPLER satellite seem to show that the hybrid phenomenon is more common than expected (Grigahcène et al. 2010; Catanzaro et al. 2010).

However, prior to arrive to firm conclusions concerning the nature of CoRoT 102699796, a more detailed theoretical

study is necessary by using a non-adiabatic oscillation code for a stability analysis of the selected modes. Furthermore the main feature of non-adiabatic codes as MAD (Dupret et al. 2003) is their ability to determine accurately the amplitudes and phases of variation of different physical quantities in the very outer layers of the stars. In particular the normalized amplitude and phase of effective temperature variations can be determined, significantly improving the accuracy of the mode identification methods through multi-band photometric approaches. An important point is that the non-adiabatic predictions are very sensitive to the modelling of the thin convective envelope of these stars and to the treatment of its interaction with pulsation, thus only time dependent convective versions of these codes would be able to reproduce both the blue and the red edge of the instability region of each mode.

## 7 DISCUSSION AND CONCLUSIONS

In this paper we presented a comprehensive study of CoRoT 102699796, a star observed by the CoRoT satellite during its first Long Run in the anticenter direction. The star was classified as  $\delta \text{ Sct}$  and shows anomalous Balmer lines at a first analysis of mid-resolution spectra obtained with GIRAFFE@VLT, thus being a likely candidate of the PMS  $\delta \text{ Sct}$  class.

We analysed the time-series photometry observed by the satellite CoRoT, detecting the presence of five independent oscillation frequencies in the range 3-6.5 c/d. These low values are somewhat atypical for PMS and “normal”  $\delta \text{ Sct}$  variables, whose peaks are usually placed around 10-30 c/d.

The star’s physical parameters were estimated on the basis of the quoted GIRAFFE@VLT mid-resolution spectra, finding that the star has spectral type F1V,  $T_{\text{eff}} = 7000 \pm 200 \text{ K}$ ,  $\log(g) = 3.8 \pm 0.4$ ,  $[M/H] = -1.1 \pm 0.2$ ,  $v \sin i = 50 \pm 5 \text{ km/s}$ ,  $L/L_{\odot} = 21_{-11}^{+21}$ . Therefore CoRoT 102699796 is the first intermediate-mass PMS pulsating star for which poor metallicity has been reported.

The evolutionary status of the target star has been explored in detail by constructing the SED, extending from the optical to the mid-infrared, using ground-based and satellite data. As a result, we find that the shape of the SED is typical of transitional circumstellar disks. Following the classification scheme of Sartori et al. (2010) for Herbig Ae/Be stars, CoRoT 102699796 can be identified as a group 2 object, i.e. between embedded objects and stars with more evolved dusty disks. Its PMS nature is reinforced by the possible association with the HII region [FT96]213.1-2.2 (Fich & Terebey 1996).

The pulsation frequencies have been interpreted in the light of the non-radial pulsation theory, using the LOSC program (Scuflaire et al. 2008) in conjunction with static and rotational evolutionary tracks calculated by means of the ATON code for stellar evolution (Ventura et al. 1998) in the standard version for asteroseismic applications with low metallicity (D’Antona et al. 2005). A minimization algorithm was used to find the model that matches the observed frequencies. As a result, either including or not the rotation, we find two possible solutions for the position of the star in the HR diagram: a) with  $\text{Log}L/L_{\odot} \sim 1.2 \div 1.3$

**Table 5.** Mode identification considering all frequencies with m=0

					$f_{obs,1}$	$f_{obs,2}$	$f_{obs,4}$	$f_{obs,5}$
					75.91	38.40	78.62	41.46
					( $\mu$ Hz)	( $\mu$ Hz)	( $\mu$ Hz)	( $\mu$ Hz)
CASE	$\chi^2$	M/M $_{\odot}$	T $_{eff}$ (K)	LogL/L $_{\odot}$	$f_{th,1}(l,n)$	$f_{th,2}(l,n)$	$f_{th,4}(l,n)$	$f_{th,5}(l,n)$
A	0.83	1.74	6850	1.21	75.89(1,-2)	38.36(2,-9)	78.67(3,-4)	41.98 <sup>3</sup> (1,-4)
B	4.92	2.29	6950	1.59	75.66(3,0)	38.57(3,-6)	78.59(2,0)	41.33(2,-3)

**Table 6.** Mode identification adding in the simulated spectra multiplet frequencies

					$f_{obs,1}$	$f_{obs,2}$	$f_{obs,3}$	$f_{obs,4}$	$f_{obs,5}$
					75.91	38.40	75.61	78.62	41.46
					( $\mu$ Hz)				
MODEL	$\chi^2$	M/M $_{\odot}$	T $_{eff}$ (K)	LogL/L $_{\odot}$	l,m,n	l,m,n	l,m,n	l,m,n	l,m,n
a1	0.28	1.84	6900	1.29	3, 1,-3	3,1,-8	3,2,-5	3,-2,-2	3,-1,-8
b1	0.37	2.28	7050	1.59	3,-1,0	3,1,-7	2,-2,0	2,-2,0	2,2,-5
b2	0.46	2.36	7000	1.63	3,-2,1	3,2,-7	2,0,0	2,1,0	2,2,3
a2	0.84	1.90	6950	1.34	3,3,-5	1,0,-3	2,1,-2	3,-1,-2	3,2,-4
b3	0.86	2.32	7250	1.62	2,1,0	2,0,-3	3,2,0	2,2,0	3,-1,-3
a3	0.88	1.83	6875	1.28	3,1,-3	1,-1,-3	2,0,-2	3,-2,-2	3,2,-15
b4	0.90	2.35	6850	1.61	2,1,0	2,0,-3	3,2,0	2,2,0	3,2,-6
b5	0.90	2.38	6950	1.64	3,-1,1	2,0,-3	3,2,0	2,2,0	2,2,-6
b6	1.00	2.36	6900	1.61	3,-1,1	2,0,-3	3,2,0	2,2,0	2,2,-6
a4	1.14	1.81	6975	1.27	2,-1,-2	1,-1,-4	3,-3,-5	3,-3,-2	3,3,-19

and M/M $_{\odot} \sim 1.8$ ; b) with LogL/L $_{\odot} \sim 1.6$  and M/M $_{\odot} \sim 2.3$ . Models with lower mass and luminosity are preferred because: i) they minimize the  $\chi^2$  and ii) their luminosities are in better agreement with the values inferred from the spectroscopically estimated logg and from the integration of the star’s SED. Finally, the model named a1 in Tab. 6 is our best-fit model (minimum  $\chi^2$  using all the five significant frequencies), having mass, effective temperature, and luminosity equal to 1.84 M/M $_{\odot}$ , 6900 K, and 1.29 LogL/L $_{\odot}$ , respectively. The position in the HR diagram of this model is in excellent agreement with the spectroscopic one. The model is very young (age $\sim 2.5$ Myr) without a convective core, in agreement with the shape of the SED that shows a significant FIR excess. The theory-observation match is based on the interpretation of frequencies  $f_1 \div f_5$  as  $g$ -modes of low-moderate n-value. To our knowledge, this is a new result and the first time that such modes are observed in PMS intermediate-mass pulsating stars. However, this is not completely surprising since it is also the first time that a so low frequency range is observed in a pulsating Herbig Ae star. In this context, it is also remarkable that CoRoT 102699796 lies in the region of HR diagram where  $\delta$  Sct and  $\gamma$  Dor instability strips intersect. Hence we are probably dealing with a star showing intermediate (hybrid) characteristics in between the two variability classes. However, we note that if the solution predicted by class a) models applied, the star could not properly be defined as an hybrid because only  $g$ -modes would be present. In this case it would be better defined as a PMS anomalous  $\gamma$  Dor star.

**ACKNOWLEDGMENTS**

We warmly thank our referee, Torsten Böhm, for his pertinent and useful comments that helped us to improve the manuscript. It is a pleasure to thank Ennio Poretti for many helpful discussions. This work was supported by the Italian ESS project, contract ASI/INAF I/015/07/0, WP 03170 and by the European Helio- and Asteroseismology Network (HELAS), a major international collaboration funded by the European Commission’s Sixth Framework Programme. This research has made use of the SIMBAD database, operated at CDS, Strasbourg, France. This publication makes use of data products from the Two Micron All Sky Survey, which is a joint project of the University of Massachusetts and the Infrared Processing and Analysis Center/California Institute of Technology, funded by the National Aeronautics and Space Administration and the National Science Foundation. Piet Reegen, author of several analysis packages used in this work, has passed away a few months ago. We wish to give our deepest sympathy to his relatives and friends.

**REFERENCES**

Auvergne, M., Bodin, P., Boissard, L., et al. 2009, A&A, 506, 411  
 Avedisova V.S. 2002, ARep, 46, 193  
 Baglin, A., Auvergne, M., Barge, P., et al. 2007, AIPC, 895, 201

- Balona, L., Ripepi, V., Catanzaro, G., Kurtz, D.W., Smalley, B., et al. 2011, MNRAS, in press
- Bernabei, S., Ripepi, V., Ruoppo, A., et al. 2009, A&A, 501, 279
- Böhm, T., Zima, W., Catala, C., Alecian, E., Pollard, K., Wright, D. 2009, A&A, 497, 183
- Böhm & Catala, 1995, A&A, 301, 155
- Breger, M. & Bischof, K. M., A&A, 2002, 385, 537
- Breger, M., Lenz, P., Antoci, V., et al. 2005, A&A, 435, 955
- Breger, M., Pamyatnykh, A. A., 1998, A&A, 332, 958
- Breger M., Stich J., Garrido R., et al. 1993, A&A, 271, 482
- Calvet, N., D'Alessio, P., Watson, D. M. 2005, ApJ, 630L, 185
- Cardelli Jason A., Clayton Geoffrey C., Mathis John S. 1989, ApJ, 345, 245
- Castelli F., Hubrig S., 2004, A&A, 425, 263
- Castelli, F., Kurucz, R. L. 2004, IAU Symp. No 210, Modelling of Stellar Atmospheres, eds. N. Piskunov et al. 2003, poster A20, also astro-ph, 045087
- Catala, C. 2003, Ap&SS, 284, 53
- Catanzaro G., Ripepi V., Bernabei S., et al. 2010, MNRAS, 411, 1167
- Chiang, E. I., Goldreich, P. 1997, ApJ, 490, 368
- Cusano, F., Ripepi, V., Alcalá, J. M., et al. 2011, MNRAS, 410, 227
- Cutri R. M., Skrutskie M. F., van Dyk S. et al , 2003, tmc book
- D'Antona, F., Cardini, D., Di Mauro, M. P., Maceroni, C., Mazzitelli, I., & Montalbán, J. 2005, MNRAS, 363, 847
- Daszynska-Daszkiwicz, J., Dziembowski, W. A., Pamyatnykh, A. A., Goupil, M.-J., 2002, A&A, 392, 151
- Debosscher J., Sarro L. M., López M., Deleuil M., Aerts, C. et al. 2009, A&A, 506, 519
- Deleuil, M., Meunier, J. C., Moutou, C. et al. 2009, AJ, 138, 64
- Delgado, A. J., Djupvik, A. A., Alfaro, E. J., 2010, A&A, 509, 104
- Di Criscienzo, M.; Ventura, P.; D'Antona, F.; Marconi, M.; Ruoppo, A.; Ripepi, V., 2008, MNRAS, 389, 325
- Dullemond, C. P., Dominik, C., Natta, A 2001, ApJ, 560, 957
- Dupret, M.-A., De Ridder, J., De Cat, P., Aerts, C., Scufflaire, R., Noels, A., Thoul, A. 2003, A&A, 398, 677
- Egan, M. P., Price, S. D., Kraemer, K. E., Mizuno, D. R., Carey, S. J., Wright, C. O., Engelke, C. W., Cohen, M., Gugliotti, M. G.: "MSX6C Infrared Point Source Catalog. The Midcourse Space Experiment Point Source Catalog Version 2.3 (October 2003)". Air Force Research Laboratory Technical Report AFRL-VS-TR-2003-1589 (2003)
- Endal, A. S., & Sofia, S. 1976, ApJ, 210, 184
- Fich, M., Terebey, S. 1996, ApJ, 472, 624
- Fumel, A., & Böhm, T. 2008, CoAst, 157, 309
- García Hernández, A., Moya, A., Michel, E., et al. 2009, A&A, 506, 79
- Gray R. O., Garrison R. F., 1989, ApJS, 69, 301
- Grigahcène, A., Dupret, M.-A., Garrido, R., Gabriel, M., Scufflaire, R. 2006, CoAst, 147, 69
- Grigahcène A., Antoci V., Balona L., et al. 2010, ApJ, 713, L192
- Guenther, D. B. & Brown, K. I. T. 2004, ApJ, 600, 419
- Guzik J.A., Kaye A.B., Bradley P.A., Cox A.N., & Neuforge C., 2000, ApJ, 542, L57
- Handler G., Shobbrook R. R., 2002, MNRAS, 333, 2, 251
- Handler G., 2008, CoAst, 159, 42
- Henry G. W., Fekel F. C. 2005, AJ, 129, 2026
- Ishihara D., Onaka T., Katata H. et al. 2010, A&A, 514A, 1
- Kallinger, T., Reegen, P., Weiss, W. W. 2008, A&A, 481, 571
- Kennelly, E. J. 1994 PhD thesis
- Kennelly, E. J., and Walker, G. A. H. 1996, PASP, 108, 327
- King H., Matthews J. M., Rowe J. F., et al. 2006, CoAst, 148, 28
- Kurtz, D. W., & Marang, F. 1995, MNRAS, 276, 191
- Kurucz R. L., Bell B., 1995, Kurucz CD-ROM No. 23. Cambridge, Mass.: Smithsonian Astrophysical Observatory.
- Kurucz R.L., 1993, A new opacity-sampling model atmosphere program for arbitrary abundances. In: Peculiar versus normal phenomena in A-type and related stars, IAU Colloquium 138, M.M. Dworetzky, F. Castelli, R. Faragiana (eds.), A.S.P. Conferences Series Vol. 44, p.87
- Kurucz R.L., Avrett E.H., 1981, SAO Special Rep., 391
- Landin N.R., Ventura P., D'Antona F., Mendes L.T.S., Vaz L.P.R. 2006, 456, 269
- Lennon D. J., Dufton P. L., Fitzsimmons A., Gehren T., Nissen P. E. 1990, A&A, 240, 349
- Lenz, P. & Breger, M. 2005, CoAst, 146, 53
- Malkov, O. Y., 2007, MNRAS, 382, 1073
- Marconi, M., & Palla, F. 1998, ApJ, 507, L141
- Mendes, L. T. S., D'Antona, F., & Mazzitelli, I. 1999, A&A, 341, 174
- Mislis, D., Schmitt, J. H. M. M., Carone, L., Guenther, E. W., Pätzold, M. 2010, A&A, 522, 86
- Moya, A. 2007, EAS, 6, 187
- Pasquini L., Avila G., Blecha A., et al. 2002, Msng, 110, 1
- Pedicelli S., Bono G., Lemasle B. et al. 2009, A&A, 504, 81
- Poretti, E., Michel, E., Garrido, R., et al. 2009, A&A, 506, 85
- Reegen, P. 2007, A&A, 467, 1353
- Reegen, P. 2010, CoAst, in press, astro-ph1006.5083
- Ripepi, V., Marconi, M., Bernabei, S., et al. 2003, A&A, 408, 1047
- Ripepi, V., Marconi, M., Palla, F. et al. 2006, Mem. Soc. Astron. It., 77, 317
- Rodríguez, E., Amado, P. J., Suárez, J. C., Moya, A., Dupret, M. A., Poretti, E., Grigahcène, A., Costa, V., López-González, M. J., 2006, A&A, 450, 715
- Rolleston, W.R.J., Dufton, P.L., Fitzsimmons A. 1994, A&A, 284,72
- Rowe J. F., Matthews J. M., Cameron C. et al. 2006, CoAst, 148, 34
- Ruoppo, V., Marconi, M., Marques, J.P. et al. 2007, A&A, 466, 261
- Russeil, D., Adami, C., Georgelin, Y. M. et al. 2007, A&A, 470, 161
- Sartori, M. J., Gregorio-Hetem, J., Rodrigues, C. V., Hetem, A., Batalha, C. 2010, AJ, 139, 27
- Scufflaire, R., Montalbán, J., Théado, S., Bourge, P.-O., Miglio, A., Godart, M., Thoul, A., Noels, A. 2008, Ap&SS, 316, 149
- Sharpless S. 1959, ApJS, 4, 257
- Skrutskie, M. F., Cutri, R.M., Stiening, R., Weinberg,

- M.D., Schneider, S. et al., 2006, AJ, 131, 1163  
Suran, M., Goupil, M., Baglin, A., Lebreton, Y., Catala, C. 2001, A&A, 372, 233  
van den Ancker, M.E., de Winter, D., Tjin, A., and Djie, H.R.E., 1998, A&A, 330, 145  
Ventura, P., Zeppieri, A., Mazzitelli, I., D'Antona, F. 1998, A&A, 334, 953  
Yamamura, I., Makiuti, S., Ikeda, N. et al. 2010, yCat, 2298, 0  
Zima, W. 2008, CoAst, 155, 17  
Zwintz K. 2008, ApJ, 673, 1088  
Zwintz, K., Hareter, M., Kuschnig, R., et al. 2009, A&A, 502, 239